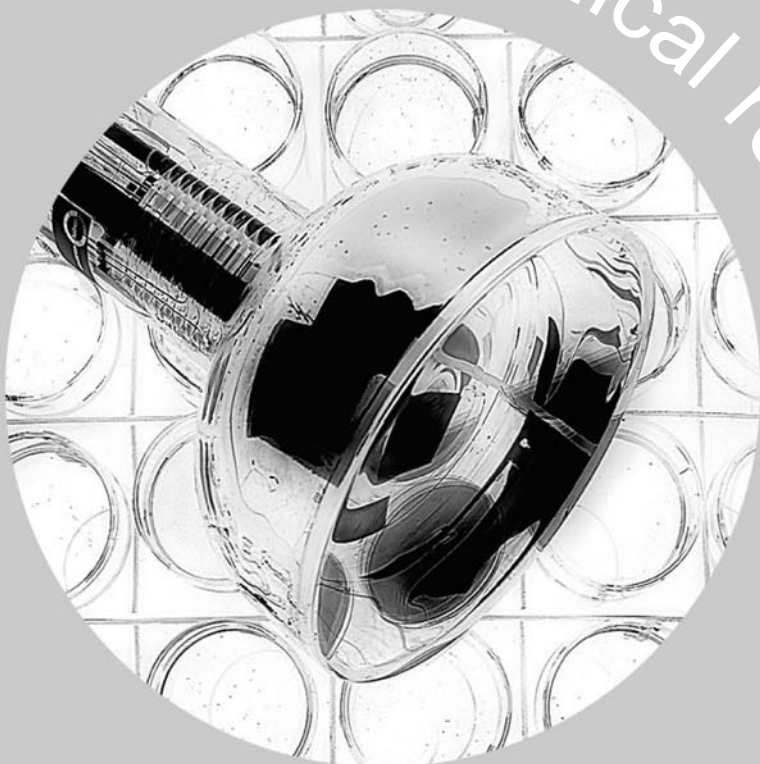


technical reprint R/P066



a comparison of current measurement  
with photon counting in the use of  
photomultiplier tubes



# a comparison of current measurement with photon counting in the use of photomultiplier tubes

C J Oliver

technical reprint R/P066

## 1 introduction

This paper compares the use of photomultipliers in the measurement of mean signal intensity and of the signal correlation function using either current-measuring or photon counting techniques.

Section 2 starts with a discussion of the different noise source introduced by photomultiplier tubes; those present in ideal tubes and extraneous noise sources introduced by sub-optimum tubes. In extracting information from the photomultiplier output some means of sampling the detector output is chosen. Different sampling schemes will be discussed in section 3.

Following this, section 4 contains an analysis of the effect of the photomultiplier noise and the sampling technique chosen on the accuracy with which information can be extracted from the measurement. This will be discussed in terms of the relative variance ( $RV$ ) of the observed quantity  $x$ , i.e.

$$RV = \frac{Var x}{\bar{x}^2} \quad \dots(1)$$

The dependence of  $RV$  on the photomultiplier noise sources and sampling scheme will be analysed in each case as a means of comparing the advantages and disadvantages of the various situations.

Section 5 gives a summary of the findings of this analysis in terms of optimum mode of operation for photomultiplier tubes in measurement of weak signals.

Finally, in section 6 the use of a photomultiplier tube in the photon counting mode of operation for the measurement of the mean intensity of a low light flux will be described as an example of the application of these principles. Factors affecting the choice of photomultiplier tube will be indicated.

It should be realised at the outset that many of the conclusions drawn are of paramount importance only when the extraction of information from very weak signals is required. If the light intensity is suf-

ficiently strong, an increase in the integration time required to obtain sufficient accuracy may well be an unimportant drawback. In the example given in section 6, as an illustration, the signal is only distinguished from the background after about 35 minutes of integration; an increase of a factor of two in the integration time could well be a major disadvantage here. This paper is, therefore, concerned primarily with achieving the ultimate sensitivity in optical measurements; not in discussing the properties which affect less critical applications.

## 2 noise sources in photomultiplier tubes

In this section the various factors which limit the performance of photomultiplier tubes in the detection of weak light fluxes and the extraction of information from them will be considered. The discussion is divided into three sections. Firstly, the noise that is introduced by the nature of the photodetection process itself is considered; secondly, that introduced by the statistical properties of the multiplication process; thirdly, extraneous noise arising from non-ideal photomultiplier tubes.

### photodetection noise

To understand photodetection it is important to realise that this is a quantum mechanical process. The intensity falling on the detector photocathode is not simply given by the classical quantity, i.e the square of the field,  $E$ .

$$I(t) = E^2(t) \quad \dots(2)$$

But by the square modulus of the position frequency component of the field (1), i.e.

$$I(t) = |E^+(t)|^2 \quad \dots(3)$$

Furthermore, it is not true to say that the detector output current is proportional to the intensity. The detector output, which makes up the fundamental data, is a train of random photodetection events, rate-modulated by the intensity. In periods of high intensity the mean photodetection rate is high whereas in periods of low intensity the rate is low, giving an apparent "bunching" of photodetections in accordance with the intensity fluctuations. Suppose one integrates the number,  $n$ , of photodetection pulses over a sample time,  $T$ , then the probability distribution,  $p(n,t)$ , will be given by (2)

$$p(n,T) = \int_0^T \frac{(\zeta l)^n}{n!} e^{-\zeta l} p(l) dl \quad \dots(4)$$

Where  $\eta$  is the photocathode quantum efficiency and  $I$  is the integral of the intensity,  $I(t)$  over the sample time, i.e.

$$I = \int_{t-T/2}^{t+T/2} I(t) dt \quad \dots(5)$$

If the intensity remains constant, **equation 4** reduces to the Poisson distribution

$$p(n, T) = \frac{\bar{n}^n}{n!} e^{-\bar{n}} \quad \dots(6)$$

Where

$$\bar{n} = \eta l$$

The “noise” is determined by the standard deviation of  $n$ , i.e.  $\sqrt{\text{var } n}$ , which is given by

$$\text{Var } n = \bar{n} \quad \dots(7)$$

for a Poisson distribution. The relative variance of the photodetection distribution is therefore, given by

$$RV = \frac{\text{Var } n}{\bar{n}^2} = \frac{1}{\bar{n}} \quad \dots(8)$$

compared with the value 0 for the intensity. The photodetection process has, therefore, led to additional “shot noise” over and above that present in the intensity fluctuations.

### multiplication noise

In addition to the photodetection shot noise a further noise source is introduced by the multiplication process occurring in a photomultiplier tube. In order to count single photodetections one requires to dominate the noise introduced by electronic components (e.g. amplifiers) following the photodetector. One needs a fast amplifier with a gain of  $10^6$  to  $10^8$  which itself introduces no noise. The electron multiplier tube is the most suitable candidate for this task so far. However, the gain process is based on multiplication by secondary emission, itself a statistical process. A primary electron bombards a dynode with an energy of about 100 eV, determined by the tube operating conditions, giving rise to several secondary electrons. The number of secondary electrons produced at each emission would be expected to have a Poisson probability distribution so that the final charge distribution at the anode,  $p(q)$ , would be a fold of many such distributions. The form of such a distribution is shown by the continuous curve in **figure 1** together with measured data points for a particular photomultiplier tube. Agreement is reasonable except that there appear to be more small pulses than the Poisson multiplication theory would predict. These observed fluctuations in the total charge per pulse arriving at the anode introduce a further source of noise over and

above photodetection noise. This excess noise is related to the normalised second moment of the charge  $q^2 / \bar{q}^2$  distribution. If we confine our attention for the moment to those photomultiplier tubes which exhibit Poisson multiplication statistics then this parameter will be given by (3).

$$\alpha = \frac{\overline{q^2}}{\bar{q}^2} \approx \frac{\mu(l-k)}{\mu-l+k} \quad \dots(9)$$

where  $q$  is the observed output charge per pulse,  $\mu$  is the secondary gain per stage, and  $k$  is that fraction of the original photodetection pulses which fail to propagate.

In practice most photomultiplier tubes do not exhibit Poisson multiplication statistics. In figure 2 the measured charge distribution from a second photomultiplier tube is compared with the Poisson multiplication prediction ( $b = 0$ , dashed curve). Various explanations have been advanced for the observed discrepancy, which is typical of most photomultiplier tubes:

- (1) variation of gain across the dynode surface.
- (2) loss of charge at the edges of the dynodes.
- (3) the existence of a large number of scattered primaries among the electrons leaving the dynodes.
- (4)
- (5)

It seems probable that a combination of all these effects will occur to a different extent in each type of tube. If we continue to restrict ourselves to the first explanation then the observed charge distribution is characterised by a further excess variance parameter,  $b$ , which lies between 0 and 1 and describes the extent to which the variance exceeds that for Poisson multiplication. In figure 2 the predicted form for  $b = 0.2$  (denoted by a full curve) shows better agreement than that for  $b = 0$ . However, as in **figure 1**, there are excess pulses of low charge tending to favour the second and third explanations, at least in the low pulse height region. Whichever explanation applies in a particular situation, the effect is to introduce a third additional noise source, corresponding to excess variance above the ideal Poisson case.

For gain fluctuations across the dynode surface the excess noise parameter  $\alpha$ , would be modified from the form of equation (9) to become

$$\alpha = \frac{\overline{q^2}}{\bar{q}^2} = \frac{\mu(b+l)(l-k)}{\mu-l+k} \quad \dots(10)$$

It should be pointed out that the fraction of pulses lost,  $k$ , increases both as the gain per stage,  $\mu$ , is reduced and as the excess variance parameter,  $b$ , is increased. These effects are illustrated in **table 1** for tubes having three different values of  $b$ , namely  $b = 0$  (Poisson multiplication, **figure 1**),  $b = 0.2$

(figure 2) and  $b = 1.0$  (worst case, exponential  $p(q)$ ). The values of  $k$  are taken from Prescott (2). In order to minimise the effects of charge fluctuations it is apparent that one must select a tube with a low  $b$  and operate at high  $\mu$ , thus minimising  $k$  and  $\alpha$ . Alternatively, one should re-standardise the output pulses using a discriminator to remove the effects of charge fluctuations. However, inevitably some of the smaller pulses will be lost below the discriminator threshold, increasing the uncertainty above that predicted for the photoelectron distribution from the cathode. Though standardisation of the output pulses reduces the excess noise, it can never improve the performance to the limiting condition occurring at the photocathode.

**extraneous noise**

An ideal photomultiplier tube would only give output pulses corresponding to annihilation of photons from the incident field. However, there are various mechanisms in photomultiplier tubes which give rise to spurious pulses and hence to additional noise. Perhaps the most basic of these, present in all tubes, is thermionic emission of dark count electrons from the photocathode, and indeed often from later dynodes. Provided that these dark counts are not correlated with signal counts or with other dark counts, they only distort the observed data by an additional flat background term. Under these conditions, corresponding to a constant dark count rate, the dark counts have a Poisson probability distribution. The fluctuations in the total dark counts will now contribute to the total uncertainty in a measurement and will become the dominant contribution

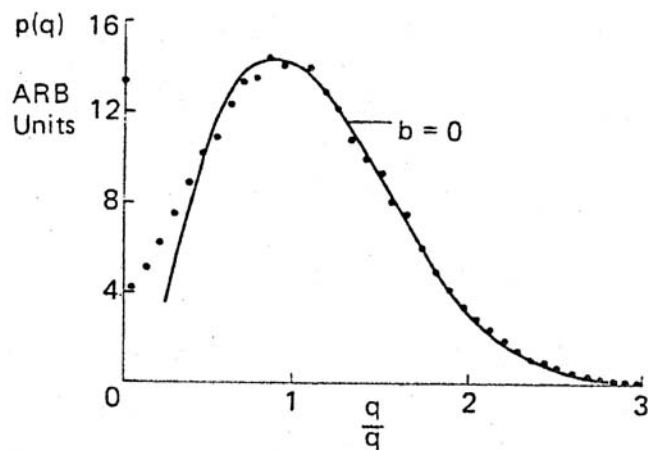


figure 1 a measured distribution of the charge per output pulse for a photomultiplier tube exhibiting near Poisson multiplication statistics. The continuous curve ( $b = 0$ ) represents the theoretical form for Poisson multiplication.

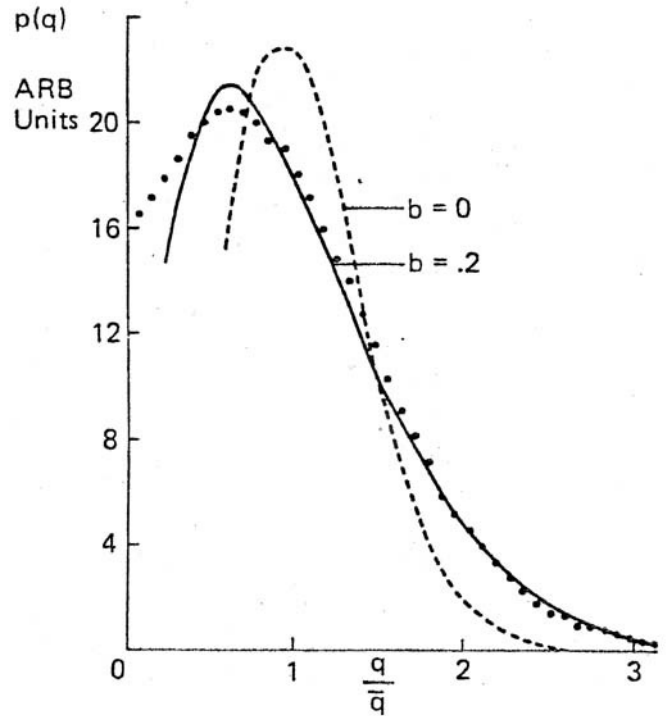


figure 2 a measured distribution of the charge per output pulse for a photomultiplier tube which does not exhibit Poisson multiplication statistics. Curves for  $b = 0$  and  $b = 0.2$  are included for comparison.

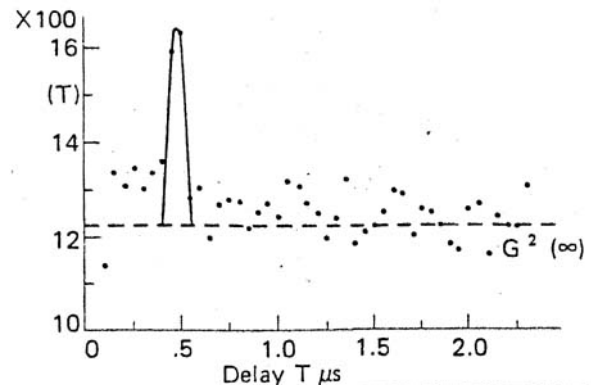


figure 3 a measured correlation function for weak coherent illumination of a photomultiplier tube exhibiting ion after pulsing.

when measuring weak signals. In addition to this inevitable dark count rate there is another source of extraneous noise associated with feedback mechanisms in the photomultiplier tube producing a second output pulse correlated with an original pulse. An example of this is shown in figure 3. Here a photomultiplier tube is illuminated by a weak light source giving a mean count rate of  $3.5 \times 10^{-4}$  counts per 50 ns sample time. The correlation function of the photomultiplier output is then measured giving the result of figure 3. For constant intensity the correlation function should lie along the dashed line at the infinite delay value  $G^{(2)}(\infty)$ . However, a distinct peak is observed centred on a delay of 480 ns probably corresponding to  $He^+$  positive ion feedback. This would seriously restrict the use of such a tube in correlation measurements and will also increase the uncertainty, as we shall see, in the measurement of intensity.

### 3 sampling techniques

In seeking to extract information from the photomultiplier output we have to select a suitable sampling technique. Suppose samples are required every  $T$  seconds. If the sampling technique consisted of measuring the signal over very narrow periods separated by  $T$ , a large number of the randomly distributed narrow photodetection pulses would be lost. Information retrieval would thus be very poor. One obviously requires some form of integration on the input signal. This is equivalent to making a narrow-band input filter (of bandwidth approximately  $1/T$ ). Two possible weighting schemes to achieve this object are illustrated in **figure 4**. Let us first consider rectangular weighting in which each pulse (here assumed standardised) is weighted with a rectangle of duration  $T$ . This is equivalent to full integration of all the pulses occurring during each sample time as can be seen by comparing the value of the weighted function at the sample time, shown in the second line of **figure 4**, with the total counts recorded during each sample time, shown in the bottom line. This method is described as photon counting when standardised pulses are used. In general I shall describe the method as full integration. If one uses and exponential weighting, arising from an RC filter, then the result is as shown in the third line of **figure 4**. Sampling the signal at each interval  $T$  obviously produces a different result from that with rectangular weighting. Used in conjunction with non-standardised photomultiplier output pulses this method is typical of current measurement techniques. There are problems associated with this type of filter, however, which must be considered. If the decay time is made too short, i.e.  $\tau_{RC} \ll T$ , the weighted function lies close to zero and the accuracy is very poor. On the other extreme, however, if the decay time is made too long, i.e.  $\tau_{RC} \gg T$ , separate samples become correlated since one can no longer follow changes in the intensity taking place on a time scale of less than  $\tau_{RC}$ . Suppose, for example, one selects a decay time  $\tau_{RC} = T/4$ , then the different samples are now only correlated by 2%. That is to say that any signal present at one sample time has decayed to 2% of its value by the next. This distortion may be acceptable in some contexts but need to be considered carefully for each situation. Ideally, one obtains the most information from a filter weighting which lies close to rectangular in both time (duration  $T$ ) and frequency (width  $B = 1/T$ ) spaces. Full integration is such a filter. This weights uniformly all data received between sample points but re-sets the total to zero at the beginning of each sample period so that each sample is independent. The operation of such

a filter can be represented by giving the integrated charge for the  $j$ th sample time i.e.

$$Q_j = \int_{t_j - \frac{T}{2}}^{t_j + \frac{T}{2}} i(t) dt \quad \dots(11)$$

Where  $i(t)$  denotes the photomultiplier output at time  $t$ . If we wish to use some arbitrary weighting function,  $h(t)$ , then the integrated charge at  $j$ th sample time would be given by

$$a_j = \int_{-\infty}^{t_j} h(t_j - t) i(t) dt \quad \dots(12)$$

For an RC filter, for example, the weighting function would be given by

$$h(\tau) = e^{-\tau/\tau_{RC}} \quad \dots(13)$$

The accuracy with which the intensity can be measured during an integration time  $NT$ , where  $N$  is the number of samples, will be determined by the accuracy with which  $Q$  can be measured.  $Q$  will be given by

$$Q = \sum_{j=1}^N Q_j \quad \dots(14)$$

with a relative variance, describing the accuracy with which  $Q$  obtained given by

$$RV = \frac{Var Q}{Q^2} \quad \dots(15)$$

If, on the other hand, we are concerned with the measurement of the correlation function at delay  $t\delta$ , defined by

$$G^{(2)}(\tau_\ell) = \sum_{j=1}^N Q_j Q_{j+\ell} \quad \dots(16)$$

The accuracy will be governed by the relative variance

$$RV = \frac{Var G^{(2)}(\tau_\ell)}{G^{(2)}(\tau_\ell)^2} \quad \dots(17)$$

### 4 the effect of the photomultiplier noise sources and the sampling technique on accuracy

Having described the various sources of noise in photomultiplier tubes it is now necessary to demonstrate the extent to which each limits the attainable accuracy in the different situation. A fuller analytical treatment will be found in reference (6) and (7) which would be consulted if more detail of the derivations is required than is given here. Throughout the present discussion I shall confine our attention to constant intensity situations. The analysis is ren-

dered somewhat more complicated if fluctuating intensities are to be considered; the principles remain the same, however.

### photodetection noise

Suppose we wish to measure the intensity during an integration time  $NT$  via the total charge as shown in equation (14). Assuming standardised photomultiplier output pulses, the relative variances for full and capacitive integration have been shown (6) to be given by rows 1 and 2 of **table 2**, where  $r$  is the count rate per second. If the capacitive integration time is chosen so the  $\tau_{RC} = NT/4$  leaving 2% correlation between samples then the relative variance with capacitive integration would be twice that for full integration. This is demonstrated in **figure 5** where a plot of the measured inverse relative variance,  $Q^2/Var Q$ , against the total counts per integration time,  $nT$ , is shown, (6). Agreement between theory, solid lines, and the experimental points confirm the validity of the theory. On measuring the correlation function, defined in equation (16), the relative variance can be shown (7) to be given by rows 3 and 5 of **table 2**. For weak signals ( $rT \ll 1$ ) the performance will be dominated by the term of order  $1/r^2T^2$ . If we select the same value of  $\tau_{RC} (=NT/4)$  as before then the relative variance for capacitive integration will be four times that for full integration implying that one would require four times longer integration time to achieve the same performance. For strong signals ( $rT \gg 1$ ), however, where performance will be dominated by the term of order  $1/rT$ , capacitive integration will require only double the integration time as full integration. The result for weak signals is demonstrated experimentally in **figure 6** in which measured correlation functions are compared for full (a) and capacitive (b) integration schemes. The count rate per second was  $r \approx 100$  with a sample time  $T = 1 \text{ ms}$ ;  $\tau_{RC}$  was selected to be 0.25 ms. The observed relative variances are 0.0011 (a) and 0.0044 (b) which is in the predicted ratio for these conditions.

Thus one would conclude that measurements using capacitive integration would typically require twice the integration time as full integration in the measurement of intensity or four times the duration in the measurement of the correlation function. As mentioned before, the excess time required could be reduced by increasing  $\tau_{RC}$  at the expense of introducing distortion in the way the observed charge follows changes in the intensity.

### multiplication noise

The effect of the fluctuations in charge has been shown (6) to give a relative variance in the measurement of total charge given by rows 5 and 6 of **table 2** for full and capacitive integration respectively. The relative variances of the correlation coefficients have been shown (7) to be given by rows 7 and 8 for full and capacitive integration respectively. The effect of charge fluctuations in the measurement of intensity is to increase the relative variance, and hence the integration time required to achieve the same performance, by  $\alpha (= \bar{q}^2/\bar{q}^2)$ . In the measurement of the correlation function the equivalent increases are  $\alpha$ , for strong signals and  $\alpha^2$ , for weak signals. In **tables 3** and **4** I compare the ratio of the required integration time  $\tau$ , for each combination of circumstances to the that required for photon-counting operation,  $\tau_o$ . A mean gain per stage of  $\mu = 5$  has been assumed with the same values of the excess variance parameter,  $b$ , and  $\alpha$  as those in **table 1**. Though the values of  $\alpha$  are derived from Prescott's analysis [3] assuming dynode inhomogeneities any experimentally derived values could equally well be used. As previously, the capacitive time constant is assumed to be  $\tau_{RC} = NT/4$ . It should be remembered that the observed anode count rate,  $r$ , is not equal to the photodetection rate at the cathode,  $r_o$ , but is reduced by the fraction of pulses that fail to propagate,  $k$ , i.e.

$$r = r_o (1-k) \quad \dots(18)$$

**table 1**

table of the dependence of  $\alpha$  and  $k$  on the values of  $b$  and  $\mu$  based on Prescott's analysis.

$b$	$\mu$	$k$	$\alpha$
0.0	4.0	0.020	1.20
	5.0	0.007	1.24
0.2	4.0	0.060	1.47
	5.0	0.034	1.44
1.0	4.0	0.200	2.00
	5.0	0.167	2.00

Further, on standardisation in a discriminator some small pulses will be lost so that the photon-counting rate is less than the true rate. The fraction lost will obviously depend on the probability of obtaining very small pulses so that it is obviously greater for the photomultiplier tube shown in **figure 2** than that in **figure 1**. In practice, a fraction between 5% and 10% of the pulses would be lost at this stage, more being lost with small  $\mu$  and large  $b$ . The results in **tables 3** and **4** thus overestimate the value of  $r_o$  in standardised operation by 5% - 10% and thus over-

estimate the disadvantage of non-standardised operation correspondingly.

**Table 3** contains the results of the measurement of intensity showing a difference of a factor 4 from best to worst cases. Generally speaking, the difference may not be significant except where very weak signals are involved. For the emasurement of correlation coefficients, as shown in **table 4**, the discrepancy is increased to a factor of 16. The use of photon-counting processing is thus more advantageous in this type of measurement. Any particular combination or filter weighting and processing method must be judged on its own merits in the light of other facts such as complexity and price, as well as ultimate performance limits.

**table 2**

The relative variance of the measured quantity under various experimental conditions.

Photomultiplier Output	Measured Quantity (X)	Integration Method	Relative Variance $\frac{Var X}{\bar{X}^2}$
Standardised	Q	Full (Photon counting)	$\frac{1}{rNT}$
		Capacitive	$\frac{1}{2\tau\tau_{RC}}$
	$G^{(12)}(\tau)$	Full (Photon counting)	$\frac{1}{N} \left[ \frac{2}{rT} + \frac{1}{r^2T^2} \right]$
		Capacitive	$\frac{1}{N} \left[ \frac{1}{r\tau_{RC}} + \frac{1}{4r^2\tau^2_{RC}} \right]$
Non-standardised	Q	Full	$\frac{\alpha}{rNT}$
		Capacitive (Current measurement)	$\frac{\alpha}{2r\tau_{RC}}$
	$G^{(12)}(\tau)$	Full	$\frac{\alpha}{N} \left[ \frac{2}{rT} + \frac{\alpha}{r^2T^2} \right]$
		Capacitive (Current measurement)	$\frac{\alpha}{N} \left[ \frac{1}{r\tau_{RC}} + \frac{\alpha}{4r^2\tau^2_{RC}} \right]$

**Figure 7** and **8** show results obtained by use of full integration for the measurement of intensity in which standardised (photon-counting) and non-standardised photomultiplier outputs were compared (6). The tube whose charge distribution was shown in **figure 2** was used with  $\mu = 6.5$ . In **figure 7** typical integrated charge distribution,  $p(Q, T)$ , are shown for standardised and non-standardised pulses when  $\bar{n} = 6.68$ . As expected the non-standardised distribution is broader. The observed relative variances for these distributions, and for other values of  $\bar{n}$  in addition, are compared with the theoretical results for photon counting in **figure 8**. The ratio of the observed to the calculated values gives a measure of  $\alpha$  for the tube. With standardised operation, the data is distributed about  $\alpha = 1.43$ , corresponding to a value for  $b$  of 0.22 in reasonable

agreement with the original charge distribution of **figure 2**. For ideal Poisson multiplication a value for  $\alpha$  of 1.19 would be expected ( $b = 0$ ) as shown, while in the worst case a value  $\alpha = 2.0$  would be expected.

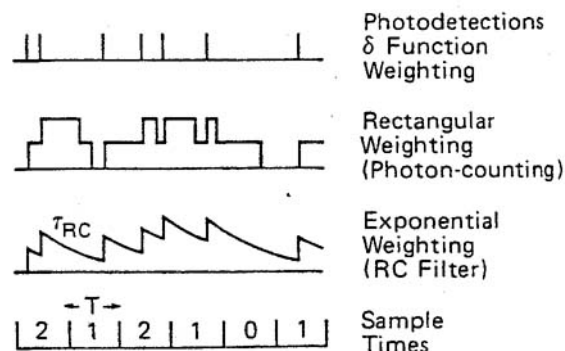


**figure 4** schematic diagram of the different sampling schemes discussed.

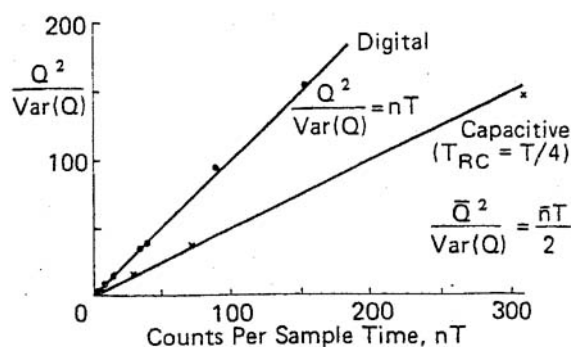


**figure 5** the dependence of the inverse relative variance of the integrated charge distributions,  $P(Q, T)$ , for standardised photomultiplier output, on the number of counts per sample time. The effect of the different storage techniques is shown. Continuous lines represent theory; the points are experimental data.

### extraneous noise

It is important to establish the extent to which extraneous pulses due to feedback mechanisms in the photomultiplier tube affect performance either by distorting the quantity being measure or by reducing the accuracy of the measurement. Having quantified the effects, one can then asses the importance of selecting tubes which are free of these defects.

### measurement of intensity

Let us initially consider the effect of correlated after pulsing on the measurement of intensity. Suppose the probability of a correlated afterpulse is  $\beta$  then  $\bar{n}_o$  original pulses will give rise to  $\bar{n}_1 = \beta\bar{n}_o$  correlated afterpulses. If only the original pulses can give rise to correlated afterpulses then in photon counting operation we have  $\bar{n}_o(1 - \beta)$  pulses with weighting one unit and  $\beta$  pulses with weighting two units. The total charge, mean and variance are then given by

$$\bar{Q}_{obs} = \bar{n}_o(1 + \beta) \quad \dots(19)$$

and

$$Var Q_{obs} = \bar{n}_o(1 - \beta) + 4\beta\bar{n}_o = \bar{n}_o(1 + 3\beta) \quad \dots(20)$$

respectively, leading to a relative variance given by

$$RV = \frac{Var Q_{obs}}{\bar{Q}_{obs}^2} \approx \frac{1 + \beta}{\bar{n}_o} \quad \dots(21)$$

This implies that a 5% correlated afterpulse probability will increase the mean observed charge by 5% and increase the integration time required to measure this quantity also by 5% compared with the ideal case. If we consider full integration of non-standardised pulses, on the other hand, we require to know the charge distribution of electrons in the secondary pulse. Let us assume that the feedback mechanism gives rise to  $f$  electrons from the cathode having a Poisson probability distribution  $p(f)$ . The final output distribution  $p(q)$  will then be the convolution of  $p(f)$  with  $p(q)$  such that

$$\frac{Var q^1}{\bar{q}^2} = \frac{Var q}{\bar{q}^2} + \frac{Var f}{\bar{f}^2} \quad \dots(22)$$

where  $q$  is the charge in an uncorrelated pulse. The mean and variance of the total observed charge can then be shown to be given by

$$\bar{Q}_{obs} = \bar{n}_o\bar{q}(1 + \beta\bar{f}) \quad \dots(23)$$

and

$$Var Q_{obs} = \bar{n}_o\alpha\bar{q}^2(1 + \beta\bar{f}^2 + \beta\frac{\bar{f}}{\alpha}) \quad \dots(24)$$

so that the relative variance is given by

$$\frac{Var Q_{obs}}{\bar{Q}_{obs}^2} = \frac{\alpha(1 + \beta\bar{f}^2 + \frac{\beta\bar{f}}{\alpha})}{\bar{n}_o(1 + \beta\bar{f})^2} \quad \dots(25)$$

Taking typical values  $\bar{f}=4$ ,  $\alpha = 1.25$  and  $\beta = 0.05$  we see that the apparent charge is overestimated by 20% and the integration time needed to obtain this quantity to a specified accuracy is increased by 36% compared with the ideal case.

It is apparent, therefore, that the presence of correlated afterpulses is unlikely to prove a major limitation, in the use of photomultiplier tubes exhibiting this phenomenon, for the measurement of light intensity.

## measurement of the correlation function

For simplicity, I shall limit the present discussion to photon-counting operation alone. The effect of charge fluctuations in the photomultiplier output when current measurement is used will serve to increase the uncertainty and distortion particularly when  $f > 1$ . The observed correlation function for a source of constant intensity is made up of two terms:

(i) the random coincidence between observed pulses which is given by

$$G_I^{(2)}(\tau) = (\bar{n}_{obs})^2 = \bar{n}_o^2(1 + \beta)^2 \quad \dots(26)$$

where  $\beta$  is the total correlated afterpulse probability formed by integrating over all delay times,  $\tau$ , i.e.

$$\hat{a} = \int_0^\infty \hat{a}(\hat{o})d\hat{o} \quad \dots(27)$$

(ii) in addition there is the correlated afterpulse term at delay  $\tau$  which is proportional to the count rate, i.e.

$$G_{obs}^{(2)}(\tau) = \beta(\tau)\bar{n}_o(1 + \beta) \quad \dots(28)$$

combining both contributions the total observed, correlation function is given by

$$G_{obs}^{(2)}(\tau) = \bar{n}^2(1 + \beta)^2 \left( 1 + \frac{\beta(\tau)}{\bar{n}_o(1 + \beta)} \right) \quad \dots(29)$$

Numerically this shows that for  $\beta = 0.05$  (as before) and  $\bar{n}_o = 10^{-3}$  the random coincidence background term would be overestimated by 10%. However, if all the correlated afterpulse probability were concentrated at a particular delay  $\tau$ , then there would be a peak at this delay 48 times greater than the background value. Referring back to the photomultiplier tube exhibiting afterpulses as shown in **figure 3** the operating conditions were that  $n = 3.5 \times 10^{-4}$ . The correlated afterpulse probability for that particular photomultiplier tube was then equivalent to  $\beta = 2 \times 10^{-4}$  only. Thus, in the measurement of the correlation function, it is important to use photomultiplier tubes which are free of afterpulsing to a very high degree. This stringent requirement on afterpulsing implies that special construction of the photomultiplier tube may be required. The example shown in **figure 3** exhibits positive ion feedback which could possibly have been reduced by modifying the design of the cathode end of the tube.

**table 3**

comparison of the effects of the different operating conditions in the measurement of the correlation coefficient for weak signals.  $\mu = 5.0$ .

photomultiplier output	integration method	excess variance (b)	$\alpha$	$\tau/\tau_\alpha$
Standardised	Full	-	1	1
	Capacitive	-	1	2
Non-standardised	Full	0.0	1.24	1.24
		0.2	1.44	1.44
		1.0	2.00	2.00
	Capacitive	0.0	1.24	2.4
		0.2	1.44	2.88
		1.0	2.00	4.00

**table 4**

comparison of the effects of the different operating conditions in the measurement of the correlation coefficient for weak signals.  $\mu = 5.0$ .

photomultiplier output	integration method	excess variance (b)	$\alpha$	$\tau/\tau_0$
Standardised	Full	-	+	1
	Capacitive	-	+	4
Non-standardised	Full	0.0	1.24	1.54
		0.2	1.44	2.07
		1.0	2.00	4.00
	Capacitive	0.0	1.24	6.2
		0.2	1.44	8.3
		1.0	2.00	16.00

**table 5**

comparison of the normalised factorial moments for coherent illumination of two different photomultiplier tubes.  $10^7$  samples were taken.

normalised factorial moment	theory	tube A	tube B
$n^2$	$1.000 + 0.001$	0.999	1.379
$n^3$	$1.000 + 0.002$	0.997	1.923
$n^4$	$1.000 + 0.003$	0.995	2.687
$n^5$	$1.000 + 0.0012$	0.990	3.819

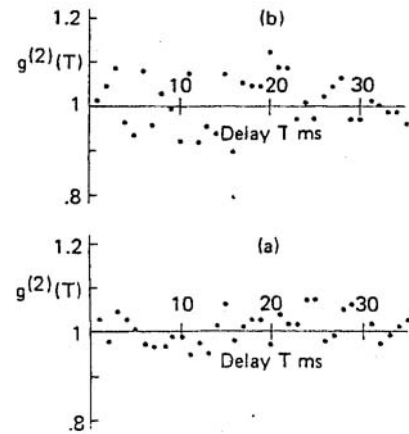


**figure 6** a comparison of (a) full integration with (b) capacitive integration in the measurement of the correlation function of a weak coherent light source. The count rate was 100 per second with a sample interval of 1 ms;  $\tau_{RC}$  was .25 ms

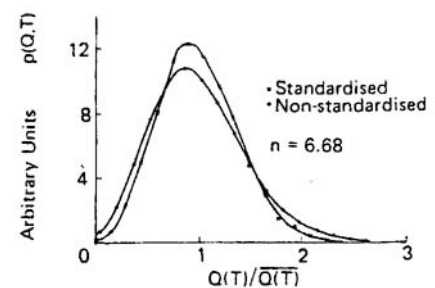


**figure 7** integrated charge distributors,  $p(Q,T)$ , showing a comparison of standardised and non-standardised operation using the photomultiplier tube as in **figure 2**.

## 5 conclusions regarding the optimum usage of photomultiplier tubes

In the preceding sections I have shown that full integration is preferable to capacitive integration for various reasons:

(i) the choice of sampling technique can introduce correlation between different samples. With full integration this problem does not arise. Filters giving rise to less correlation between samples than the RC filter described here can, of course, be designed. It is not possible, however, to improve on the full integration performance.

(ii) allied with the previous conclusion is the finding that the existence of correlations between samples forces one to use a filter profile of greater bandwidth which increases the experimental uncertainty to an extent determined by the basic filter shape and the acceptable correlation level.

(iii) a third advantage of full integration that has not previously been mentioned is that the choice of filter response is automatically linked to the separation of samples. Other filters require separate adjustment for each sample interval.

The advantage of standardised operation in removing noise due to variation in charge from pulse to pulse was also demonstrated. If full integration and standardised pulse operation are combined in photon-counting operation we obtain the best performance for a given photomultiplier tubes. Accuracy in the measurement is greatest and the effect of correlated afterpulsing is reduced; particularly if the afterpulses are large compared with the original pulses. The effect of correlated afterpulses in general is less damaging in the measurement of intensity than in the measurement of the correlation function. It was shown to be essential to select a photomultiplier tube with very low afterpulse probability in the latter case to avoid significant distortion of the correlation function at certain particular delay-times. The existence of such correlated afterpulses does not significantly distort the mean value of the intensity and serves merely to increase the integration time required for a given accuracy.

## 6 the measurement of low light flux by photon-counting

To illustrate some of the points raised so far I shall finish by discussing the application of these principles to the measurement of low light flux (8). For reasons already given one uses the technique of photon-counting. The first step is to select a suitable photomultiplier tube. I shall illustrate this procedure with a comparison of three different photomultiplier tubes having nominally similar specifications. In order to establish whether the tubes are free of afterpulsing the photon-counting probability distributions,  $p(n, T)$ , were studied. For a constant intensity source, as shown in equation (6), the distribution should be Poisson, characterised by having normalised factorial moments given by

$$n^{(r)} = \langle n(n-1)\dots(n-r+1) \rangle / n^r = 1 \quad \dots(30)$$

This measurement is an alternative to measurement of the correlation function leading to an excess variance if afterpulsing occurs. The afterpulse probability,  $\beta$ , is related to the observed normalised second factorial moment by

$$\beta = \frac{\bar{n}}{2} (n^{(2)} - 1) \quad \dots(31)$$

Initially tubes A and B were illuminated by laser light, their photon-counting distributions were measured and their factorial moments calculated as shown in **table 5**. It is apparent that tube B is introducing excess noise due to correlated afterpulses and can be rejected. Since we are concerned with the measurement of low light flux we shall be primarily limited by the properties of the detector dark

counts. In **table 6** the results of photon-counting statistics measurements (9) of the room temperature and cooled dark-counts for tubes A and C are shown. At room temperature both tubes give acceptable performance but on cooling tube A gives evidence of ~20% correlated afterpulse probability. This tube also can be eliminated leaving tube C as the suitable photomultiplier for low light level work. In measuring low light levels one uses the method of synchronous detection (8) in which one spends equal intervals of time recording dark-counts alone and dark-counts plus signal. To remove the effects of systematic drifts it is best to operate by integrating over many alternate periods of the two states. Suppose we record the total dark counts only as  $n_1$ , the signal plus dark counts as  $n_2$  and the next dark counts as  $n_3$ . The signal can be obtained from the difference estimator.

$$\hat{S} = n_2 - n_1 \quad \dots(32)$$

while taking the difference between pairs of dark-count measurements gives a background estimator,

$$\hat{B} = n_1 - n_3 \quad \dots(33)$$

The mean values of these estimators are given by

$$\langle \hat{S} \rangle = \frac{r_s T}{2} \quad \dots(34)$$

and

$$\langle \hat{B} \rangle = 0 \quad \dots(35)$$

where  $r_s$  is the signal count rate per second. Their variances are given by

$$Var \hat{S} = \frac{r_s T}{2} + r_d T \quad \dots(36)$$

and

$$Var \hat{B} = r_d T \quad \dots(37)$$

where  $r_d$  is the detector dark-count rate per second.

In **figure 9** the evolution of these two estimators with time is shown as they are progressively summed. The data points perform a random walk about their mean values generally lying inside the standard deviation. ( $\sqrt{Variance}$ ) parabolae also included in the diagram. The mean light flux was found to be 0.043 counts per second against a cooled dark-count rate of 0.459 per second. After 35 minutes of integration the two quantities become effectively resolvable. Obviously, measurement of such weak signals ( $\sim 6.3 \times 10^{-17} W$ ) requires the optimum choice of detector and experimental technique to avoid excessive integration time. This

type of light level is not untypical of that encountered in some classical spectroscopy of astronomical situations.

### references

- [1] R J Glauber, 1963, Phys.Rev.Letts., 10, 84
- [2] L Mandel, 1959, Proc.Phys.Soc.(London), 74, 233
- [3] J R Prescott, 1966, Nucl.Intrum.Meths, 39 173
- [4] P B Coates, 1970, J.Phys.D,3, 1290
- [5] P B Coates, 1973, J.PhysD, 6, 153
- [6] R Jones, C J Oliver and E R Pike, 1971, Appl.Opts., 10, 1673
- [7] Chapter by C J Oliver in "Photoncorrelation and light beating Spectroscopy", eds. H Z Cummins and E R Pike (Plenum, New York, 1974)
- [8] C J Oliver and E R Pike, 1968, J.Phys. D., 1, 1459
- [9] R Foord, R Jones, C J Oliver and E R Pike, 1969, Appl.Opts., 8, 1975

### acknowledgements

The author wishes to acknowledge his indebtedness to the publishers for permission to reproduce the following figures:  
 Applied Optics: figures 1, 2, 5, 7; reference [6].  
 Plenum, New York: figures 3, 6, 8; reference [7].  
 Institute of Physics, J.Phys.D: figure 9; reference [8].

**table 6** comparison of the normalised factorial moments for the dark counts of two different photomultiplier tubes. At room temperature  $10^5$  samples were taken; when cooled  $10^4$  samples were taken for tube A and  $10^3$  samples for tube C.

normalised factorial moment	room temperature			cooled			
	theory	tube A	tube C	theory	tube A	theory	tube C
$n^2$	1.000 + 0.009	1.009	1.000	1.00 + 0.03	1.73	1.00 + 0.09	1.01
$n^3$	1.000 + 0.017	1.034	0.999	1.00 + 0.05	6.85	1.00 + 0.17	1.02
$n^4$	1.000 + 0.030	1.088	0.991	1.00 + 0.10	9.94	1.00 + 0.30	0.97
$n^5$	1.000 + 0.12	1.205	0.97	-	-	-	-

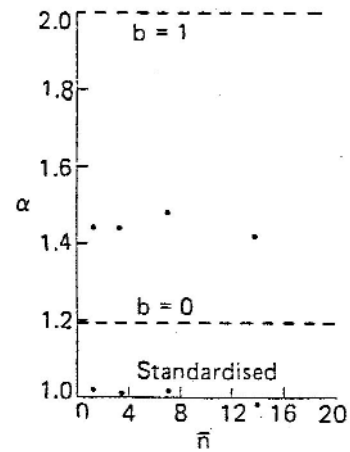


**figure 8** the dependence of  $\alpha = \overline{q^2}/\overline{q}^2$  on output standardisation for different numbers of counts per sample time for the photomultiplier as in **figure 2**.

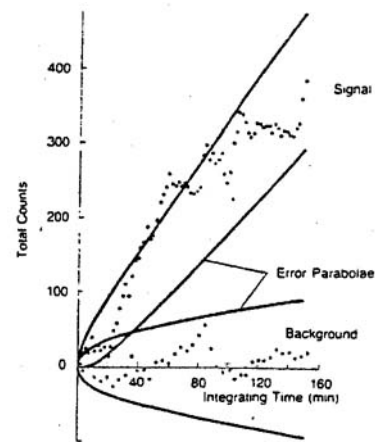


**figure 9** random walks of the signal and background estimators in the measurement of a low light flux by synchronous detection.

**Electron Tubes Limited**

Bury Street, Ruislip

Middx HA4 7TA, UK

Tel: +44 (0)1895 630771

Fax: +44 (0)1895 635953  
35953

Email: [info@electron-tubes.co.uk](mailto:info@electron-tubes.co.uk)

**Electron Tubes Inc.**

100 Forge Way, Unit F

Rockaway, NJ 07866, USA

Tel: (973)586 9594

Toll free: (800)521 8382

Fax: (973)586 9771

Email: [sales@electrontubes.com](mailto:sales@electrontubes.com)

[www.electrontubes.com](http://www.electrontubes.com)

**Contact us today we have a  
world-wide network of agents  
and distributors.**

talk to us about your  
application or choose a product  
from our literature:

photomultipliers & voltage dividers

light detector assemblies

electronic modules

housings

X-ray detector modules

power supplies